



Subsurface migration of H₂O at lunar cold traps

Norbert Schorghofer¹ and G. Jeffrey Taylor²

Received 22 June 2006; revised 14 September 2006; accepted 13 October 2006; published 23 February 2007.

[1] Permanently shaded areas near the poles of the Moon and Mercury may harbor water ice. We develop a physical model for migration of water molecules in the regolith and discover two pathways that can lead to accumulation of H₂O in the subsurface. A small fraction of water molecules delivered, either continuously or abruptly, to permanently cold areas diffuses into the regolith and can remain there longer than on the surface. Higher temperatures lead to deeper burial. At constant temperature, this diffusive migration produces less than one molecular layer of volatile H₂O on grains, because it is driven by differences in surface concentrations. The water is therefore expected to be in adsorbed form, and the amount stored in this fashion could be at most a few hundred ppm of H₂O. A second pathway is pumping by diurnal temperature oscillations from a transient ice cover that may have formed during a large comet impact. It can lead to high ground ice densities, but the ground ice layer lasts not long beyond the disappearance of the ice cover. Both types of subsurface charging mechanism work best for temperatures typical of permanently shaded areas with sunlit surfaces in their field of view.

Citation: Schorghofer, N., and G. J. Taylor (2007), Subsurface migration of H₂O at lunar cold traps, *J. Geophys. Res.*, 112, E02010, doi:10.1029/2006JE002779.

1. Introduction

[2] Water molecules delivered to the Moon or Mercury from space transiently move along ballistic trajectories and can get trapped at permanently shaded areas near the poles, where sublimation rates are so low that ice would survive over billions of years [Watson *et al.*, 1961a, 1961b; Arnold, 1979, 1987; Svitek and Murray, 1988; Vondrak and Crider, 2003]. After H₂O molecules have arrived on the surface of cold traps, they can continue to hop into the regolith. Transport and deposition of water molecules has been studied previously. To transport and trapping, we add subsurface migration caused by molecular diffusion in the porous regolith, taking a different approach than that used by Cocks *et al.* [2002].

[3] Permanently shaded areas near the lunar poles have not seen the sun for at least 2 billion years [Ward, 1975]. Volatiles are delivered to the Moon and Mercury by comets, meteoroids, interstellar dust particles, and solar wind. Estimates reach 10¹⁴ kg over 2 × 10⁹ years for the Moon [Arnold, 1979], but are uncertain. Furthermore, many of the molecules are destroyed by photodissociation on their way to the cold traps. Moses *et al.* [1999] estimate up to 6 × 10¹⁴ kg of water was delivered to Mercury over 3.5 billion years by micrometeorites. The ice that arrives in cold areas may last billions of years. As calculated below,

the sublimation loss at 100 K is $E \approx 1 \text{ kg m}^{-2}\text{Ga}^{-1}$, the equivalent of a 1 mm thick layer in 1 billion years.

[4] Ice is lost not only by sublimation, but also by UV-radiation from the sun or the local interstellar medium [Morgan and Shemansky, 1991] and by sputtering from solar wind directly or from the tail of Earth's magnetosphere [Lanzerotti *et al.*, 1981]. The destruction rates may exceed accumulation rates [Lanzerotti *et al.*, 1981], which questions whether ice really exists in the cold traps.

[5] Observationally, there is evidence for and against ice in permanently shaded areas on the Moon [Stacy *et al.*, 1997; Feldman *et al.*, 1998]. Lawrence *et al.* [2006] report 100–150 ppm of hydrogen near both poles measured with the Lunar Prospector neutron spectrometer, compared to 50 ppm at more equatorial latitudes. A bistatic radar experiment by Clementine also suggested the presence of water ice [Nozette *et al.*, 1996]. On the other hand, radar observations of areas visible from the Arecibo radar antenna indicate no unambiguous evidence for water ice in lunar permanently shadowed regions [Campbell *et al.*, 2003]. In contrast, there is radar evidence for the presence of ice at the poles of Mercury [Slade *et al.*, 1992; Butler *et al.*, 1993; Harmon *et al.*, 1994].

[6] Ground ice would be better protected from destruction by space weathering than exposed ice. Crider and Vondrak [2003a, 2003b] have modeled burial by impact ejecta. We take a different approach. Section 2 describes the physical concepts that govern migration within extremely cold regolith in a vacuum environment. Previous studies [Watson *et al.*, 1961b; Arnold, 1979; Butler *et al.*, 1993; Butler, 1997] describe lateral migration to cold traps. The ratio of time of flight to residence time is large for ballistic hops on the dayside, but tiny in the pores of permanently shaded areas. Migration of inert gases is limited by diffusion through

¹Institute for Astronomy and NASA Astrobiology Institute, University of Hawaii, Honolulu, Hawaii, USA.

²Hawaii Institute of Geophysics and Planetology and NASA Astrobiology Institute, University of Hawaii, Honolulu, Hawaii, USA.

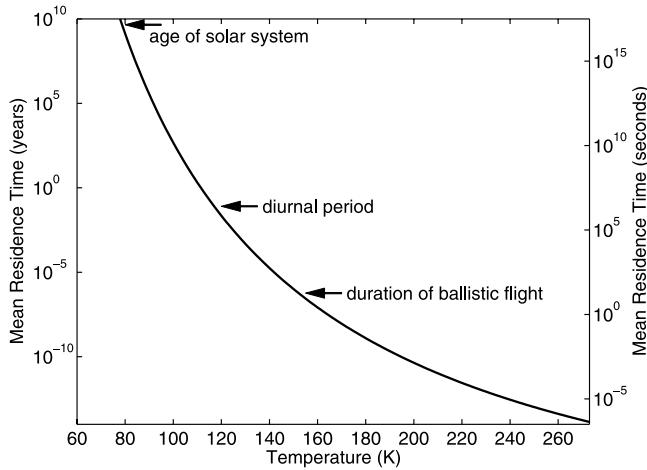


Figure 1. Mean residence time τ of water molecules on crystalline ice as a function of temperature. The diurnal period and the duration of a typical ballistic flight on the Moon are also indicated.

grains, as studied by *Killen* [2002], in contrast to transport in intergrain pores, considered here. In section 3 quantitative equations for subsurface migration are developed. Section 4 contains analytical solutions to these equations for constant temperature; we consider the survival time of buried ice and deposition of water by large comet impacts and by continuous delivery to the cold trap. Section 5 discusses the role of impact gardening and adsorption. Sections 6 and 7 deal with multilayer coverage and time varying temperature. The last section summarizes the results.

[7] This work is mainly relevant to the Moon. The likely pure ice deposits on Mercury do not call for a mechanism that can at most fill pore spaces with ice. Yet the results apply equally to Mercury, and the results on outward migration furthermore to comets and minor bodies when ice is lost through a porous layer.

2. Physics of Vapor Migration

[8] Here we develop a physical model for molecular diffusion at low temperature in an exosphere. To begin with, we rederive the expression for the sublimation rate of ice in vacuum. The rate of incident particles from a saturated atmosphere is [*Langmuir*, 1913; *Watson et al.*, 1961b]

$$E_{\max} = P_v / \sqrt{2\pi kT\mu}, \quad (1)$$

with P_v the equilibrium vapor pressure, k the Boltzmann constant, T temperature, and μ the mass of an H₂O molecule. This is a maximum condensation rate, because not all incident molecules stick to the surface. A fraction $(1 - \alpha)$ of incident molecules is reflected from the surface, where α is the condensation coefficient. For ice, the coefficient α in the temperature range 40–120 K is in the range 1–0.7 [*Haynes et al.*, 1992].

[9] The saturation vapor pressure P_v is defined by an equilibrium between particles that hit the surface and stick to the surface and the number of molecules that escape from

a solid ice surface. When vapor is in equilibrium with ice, the evaporation rate equals the condensation rate,

$$E_{\text{condensation}} = \alpha E_{\max} = E_{\text{evaporation}}. \quad (2)$$

The evaporation or sublimation rate is also applicable without atmosphere. It may appear counterintuitive that the sublimation loss into vacuum depends on the saturation vapor pressure P_v even when no vapor is present. The equilibrium pressure is defined by a balance between incoming and outgoing flux, and it encodes the energy barrier a molecule has to overcome to escape. This energy barrier is the same with or without the presence of vapor. Throughout this paper we abbreviate $E_{\text{evaporation}}$ with E .

[10] At any nonzero temperature, molecules have a probability to leave the surface they are bound to. The mean residence time τ of a molecule is $\tau = \theta/E$, where θ is the number of molecules per area. The areal density of H₂O molecules for solid ice is $\theta = (\rho/\mu)^{2/3}$, where ρ is the density of solid ice. The numerical value is $\theta \approx 10^{19}$ molecules/m². In summary, the residence time of a molecule, in the absence of other loss mechanisms, is

$$\tau = \frac{\theta}{E} = \frac{\theta}{\alpha E_{\max}}. \quad (3)$$

[11] Figure 1 shows the residence time of water molecules as a function of temperature. It assumes a simple form for P_v ,

$$P_v = p_t \exp\left[-\frac{Q}{k}\left(\frac{1}{T} - \frac{1}{T_t}\right)\right], \quad (4)$$

where p_t and T_t are the triple point pressure and temperature and $Q = 51.058$ kJ/mol is the sublimation enthalpy. Below roughly 150 K, the molecules spend most of their time residing on the surface and a comparatively short time on ballistic jumps. This intuitively matches earlier concepts of molecules that hop at high temperatures on the dayside of the Moon, but do not hop at low temperatures on the nightside or in permanently shaded areas [*Arnold*, 1979; *Butler*, 1997]. Our physical model provides finite residence times at all temperatures and can describe the migration of H₂O molecules within cold areas.

[12] Experimentally measured sublimation rates for H₂O ice are shown in Figure 2. *Sack and Baragiola* [1993] measured sublimation rates between 135 and 170 K, and rates near 135 K for films deposited and grown at lower temperatures. Below 140 K, fresh films have enhanced sublimation rates attributed to sublimation from regions containing amorphous ice. Precise rates depend not only on temperature, but also on history. *Bryson et al.* [1974] determined sublimation rates between 132 and 187 K, noticing a transition around 150 K. Data from the International Critical Tables [*Washburn et al.*, 2003] above -90°C are based on earlier experiments.

[13] The binding energy of molecules adsorbed to the regolith or on amorphous ice differs from that in crystalline ice [*Speedy et al.*, 1996]. H₂O deposited at very cold temperatures is expected to form amorphous ice. In the light of other uncertainties, we use equation (4), which closely follows that from the International Critical Tables, as

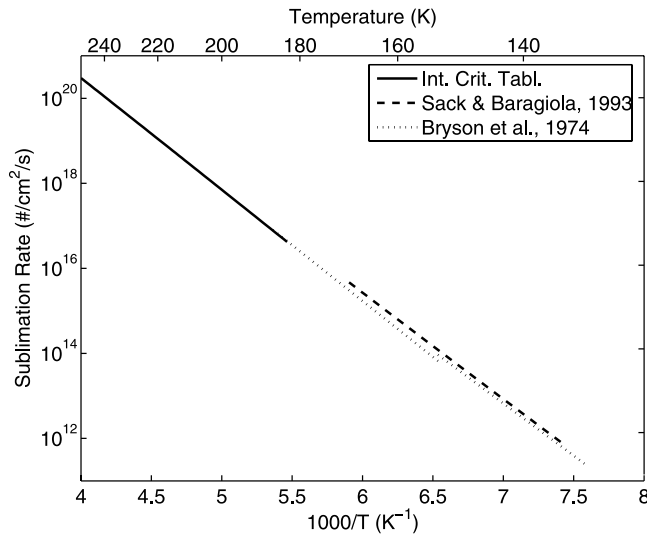


Figure 2. Experimental evaporation rates for ice in units of number of molecules per area and time.

a description of the saturation pressure in section 4. Physically adsorbed H₂O is discussed in section 5.

3. Subsurface Migration

3.1. Statistical Model

[14] Water molecules on the surface can migrate into the porous, loose regolith by random jumps. The mean grain size in lunar soil samples is typically 45–100 μm [Heiken *et al.*, 1991]. Our model uses discrete jumps of length $\ell = 75 \mu\text{m}$, which represent a typical grain size diameter, assumed to approximate pore space size. The model involves one spatial dimension, the vertical. The temperature is assumed to be constant with time and increases linearly with depth, $T(z) = T(0) + gz$, where g is the geothermal gradient.

[15] The first type of model is a statistical simulation of individual molecules. At every time step of duration Δt , there is a probability $\Delta t/\tau$ for the molecule to leave the surface. Once released we assume molecules move with equal probability upward or downward. Molecules that move upward from the surface are assumed lost. Also, there is a probability $(1 - \alpha)$ that molecules reflect immediately rather than stick.

[16] Model calculations are carried out with a continuous supply of water molecules to the surface of a cold trap. Figure 3 shows the number of H₂O molecules in the ground as a function of time. Only a fraction of the water supplied accumulates in the subsurface, most is lost from the surface, but the amount of H₂O steadily increases with time. Lower temperatures favor retention of water, but higher temperatures lead to deeper burial (not shown). (The dependence of the model results on various parameters will become clear later, when we solve the model analytically.)

[17] Molecular random walk leads to diffusive migration and we now obtain the corresponding diffusion coefficient. The probability to end up at a distance $j\ell$ after n hops is given by a binomial distribution,

$$p(j) = \frac{1}{2^n} \frac{n!}{\binom{n-j}{2} \binom{n+j}{2}!}$$

where $-n \leq j \leq n$ (either all odd or all even). This leads to a mean-square displacement of

$$\langle z^2 \rangle = \sum_j (\ell j)^2 p(j) = \ell^2 n.$$

One hop requires τ time, and n hops require $n\tau$ time. Hence the mean-square displacement is $\langle z^2 \rangle = \ell^2 t/\tau$. For a point source that spreads according to the diffusion equation $\langle z^2 \rangle = 2Dt$. Hence the diffusion coefficient is

$$D = \ell^2 / (2\tau). \quad (5)$$

In this derivation, we have neglected the probability that a molecule immediately jumps a second time, that is, the sticking coefficient α is assumed to be 1.

3.2. Continuum Description

[18] The migration process can also be described in terms of a continuous mass density $\rho(z, t)$. The outward flux from any site is σ/τ , where σ is the areal density. The net flux of molecules between two neighboring subsurface sites at depth z_n and $z_{n+1} = z_n + \ell$ is

$$J_{n \rightarrow n+1} = -\mu \left(\frac{\sigma_{n+1}}{2\tau_{n+1}} - \frac{\sigma_n}{2\tau_n} \right) = -\mu \ell \frac{\partial}{\partial z} \left(\frac{\sigma}{2\tau} \right)_n.$$

The factor of 2 in the denominator appears, because a molecule can leave in one or the other direction. Mass density and surface density are related by $\rho = \mu\sigma/\ell$. The flux at any depth is therefore

$$J = -\frac{\ell^2}{2} \frac{\partial}{\partial z} \left(\frac{\rho}{\tau} \right). \quad (6)$$

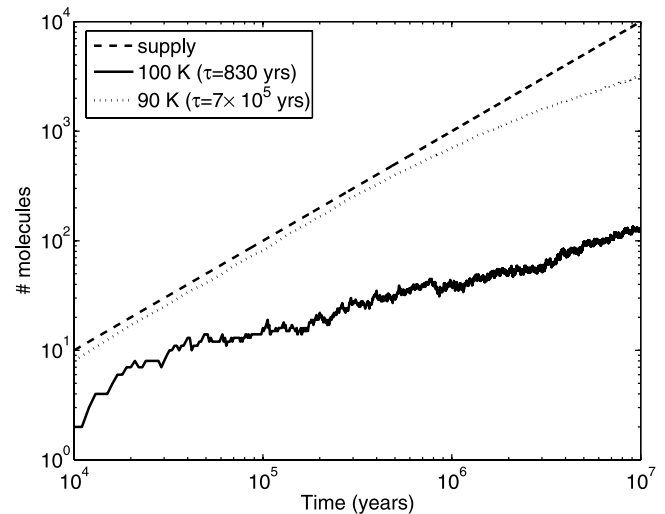


Figure 3. Statistical model calculations of H₂O migration into the subsurface with a continuous supply of water molecules to the surface. The graphs show the amount of subsurface ice as a function of time for two temperatures. Only a fraction of the water supplied accumulates in the subsurface; most is lost from the surface, but the amount of H₂O steadily increases with time. The number of supplied molecules is small for computational convenience and is much higher in reality.

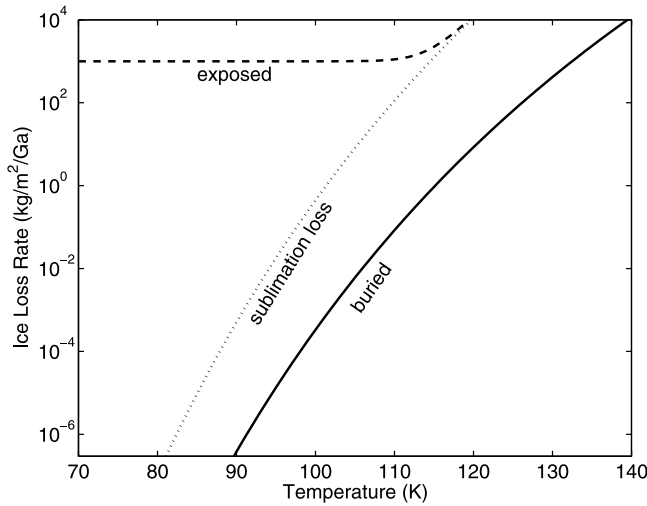


Figure 4. Loss rate of ice on the surface (dash line) and buried beneath a 10 cm thick layer of 75 μm large grains (solid line). The total loss rate for exposed ice consists of a temperature independent space weathering rate and a temperature dependent sublimation loss rate (dot line).

Local mass conservation dictates $\partial\rho/\partial t + \partial J/\partial z = 0$. Hence the mass density evolves according to

$$\frac{\partial\rho}{\partial t} = \frac{\ell^2}{2} \frac{\partial^2}{\partial z^2} \left(\frac{\rho}{\tau} \right). \quad (7)$$

[19] If the temperature is constant with depth, then the residence time can be pulled out of the derivative, and the migration is described by the diffusion equation

$$\frac{\partial\rho}{\partial t} = D \frac{\partial^2\rho}{\partial z^2} \quad (8)$$

with a diffusion coefficient of $D = \ell^2/(2\tau)$. This is the same coefficient we derived above based on the random walk model, equation (5). Note that the diffusion equation arises not because one gas diffuses through another, but from random migration of a single molecule species.

[20] When geothermal heating is not neglected, expansion of equation (6) yields

$$\begin{aligned} J &= -\frac{\ell^2}{2\tau} \frac{\partial\rho}{\partial z} - \frac{\ell^2}{2} \rho \frac{\partial}{\partial z} \frac{1}{\tau} \\ &= -D \frac{\partial\rho}{\partial z} + w\rho \\ &= J_{\text{diff}} + J_{\text{geo}} \end{aligned} \quad (9)$$

The first term on the right-hand side is a diffusive flux; the second term is an advective flux with an outward velocity w , due to a temperature increase with depth. The thermal conductivity of the most surficial layer on the Moon can be extremely low, and the temperature increase with depth correspondingly large [Heiken *et al.*, 1991].

[21] The derivative of τ with respect to depth z depends on the geothermal temperature gradient $g = \partial T/\partial z$. With the expression from equation (4),

$$\frac{\partial}{\partial z} \left(\frac{1}{\tau} \right) = \frac{g}{\tau T} \left(\frac{Q}{kT} - \frac{1}{2} \right).$$

The ratio of advective to diffusive flux at any time is

$$\frac{J_{\text{geo}}}{J_{\text{diff}}} = \frac{\rho \partial(1/\tau)/\partial z}{(\partial\rho/\partial z)/\tau} \approx \frac{Zg}{T} \left(\frac{Q}{kT} - \frac{1}{2} \right), \quad (10)$$

where Z is the length-scale over which ρ changes significantly. The geothermally induced flux becomes important when the relative change in temperature due to geothermal heating, Zg/T , becomes comparable to $1/(Q/kT - 1/2) \approx 0.02$. For a gradient of $g = 1$ K/m, this occurs at a depth of about 2 m.

4. Solutions to the Subsurface Migration Model

[22] The general continuum equation (7) can now be solved. In fact, we only solve the simpler equation (8) and are subject to the limitation from the geothermal temperature gradient described by equation (10). Throughout this section, we take the temperature to be constant in time.

4.1. Loss Rate of Buried Ice

[23] The first of several applications is the determination of the survival time of ice buried by a layer of regolith of thickness Δz . Obviously, buried ice lasts substantially longer than ice on the surface, because a molecule has to undergo many hops to escape. Our physical model allows us to determine its life time.

[24] The flux at the upper boundary of the ice layer is given by $J = -D\partial\rho/\partial z$. Assuming the amount of ice at question is much larger than could be buffered by partially “wetted” grains in the overlying dry layer, a linear density profile will be established after a transient period, that is, equation (8) evolves toward $\partial^2\rho/\partial z^2 = 0$. Thereafter, $\partial\rho/\partial z$ is constant and the density gradient is determined by the difference between the surface density (essentially zero) and the density at the ice-regolith boundary ($\mu\theta/\ell$). The loss rate is given by

$$J = D \frac{\mu\theta}{\ell\Delta z} = \frac{\mu\ell\theta}{2\tau\Delta z} = \frac{\mu\ell E}{2\Delta z}. \quad (11)$$

Figure 4 shows this loss rate for ice buried beneath a 10 cm thick layer, compared to the loss rate of exposed ice. The total loss rate for exposed ice consists of a temperature independent space weathering rate, δ , and a temperature dependent sublimation loss rate, E .

[25] A subtle but important point in the derivation of this formula is that ρ in the immediate vicinity of the ice is $\mu\theta/\ell$, which is much smaller than the bulk density of solid ice, because ℓ is much larger than the size of an H₂O molecule. The first layer of grains on top of the ice layer receives a certain flux from the ice and must send back less than it receives to maintain its transport capability. The grains maintain less than a complete layer of volatile H₂O mole-

cules, and the interstitial voids are not filled at a higher density of H₂O.

[26] A dry layer has two important effects on the survival time of buried ice, in addition to the protection from space weathering it provides. It lowers the peak temperature experienced by the ice, which can be very important [Vasavada *et al.*, 1999; Harmon *et al.*, 2001], but this effect is not included in the constant temperature calculations here. Figure 4 shows the effect of the diffusive barrier the water has to migrate through. For time varying temperature, equation (11) generalizes to,

$$\langle J \rangle = \frac{\mu \ell}{2\Delta z} \langle E(\text{at ice-regolith boundary}) \rangle, \quad (12)$$

where angular brackets indicate the time average. The damping of temperature cycles by the overlying layer can result in a dramatic reduction of $\langle E \rangle$ at the ice-regolith boundary relative to $\langle E \rangle$ on the very surface.

[27] Equation (11) is equivalent to the Knudsen flow through a porous medium. The Knudsen diffusion coefficient is on the order of $D_K = K \bar{v} \ell$, where \bar{v} is the mean thermal velocity of molecules $\bar{v} = \sqrt{(8/\pi)kT/\mu}$ and K a geometry dependent constant of order one. The flux is $J_K = D_K \Delta \rho' / \Delta z$, where ρ' is not the total density of H₂O, but the density of H₂O in the gaseous phase. From the ideal gas law $\rho' = \mu P / (kT)$, where P is pressure. The Knudsen flux is, using equation (1),

$$J_K = K \sqrt{\frac{8kT}{\pi\mu}} \frac{\mu P_v}{kT} \frac{\ell}{\Delta z} = 4K \frac{\ell}{\Delta z} \mu E_{\text{max}}.$$

This agrees with equation (11) within a prefactor. The flux is reduced relative to sublimation from an exposed ice surface by a factor of order $\ell/\Delta z$. Knudsen flux calculations have been used for comets, the Moon, and Mercury by, e.g., Fanale and Salvail [1984] and Salvail and Fanale [1994]. The ideal gas vapor density at low temperatures is so small that a pore space usually does not contain even a single molecule, yet the Knudsen formula turns out to be applicable.

4.2. Slow Continuous Water Delivery

[28] Here we consider the accumulation of subsurface H₂O due to slow but steady supply of water molecules to the cold trap. Slow means the supply rate is less than the loss rate, so that the surface is never fully covered with H₂O molecules. If σ_0 denotes the areal density of H₂O molecules on the surface, then $\sigma_0 \leq \theta$. From the surface, molecules are lost to sublimation at rate $\sigma_0/(2\tau)$. The sublimation rate is taken to be half of that of bulk ice, because the other half migrates at least one step into the subsurface and about as much comes back. This factor of 2 is, in any case, unimportant for order of magnitude estimates. The space weathering rate is assumed to be proportional to the fraction of surface area covered with H₂O molecules σ_0/θ , because only a fraction of hostile particles hit H₂O molecules.

[29] The balance of H₂O molecules on the surface is described by

$$\frac{\partial \sigma_0}{\partial t} = s - \frac{\sigma_0}{2\tau} - \frac{\sigma_0}{\theta} \delta, \quad (13)$$

where σ_0 is the areal density of H₂O molecules on the surface (number of molecules per area), s the rate of continuous H₂O supply, θ the areal number density of H₂O molecules for solid ice, and δ the destruction rate from space weathering. As will become apparent below, the net flux of molecules into the subsurface is relatively small and can be neglected in (13). Even when the space weathering rate exceeds the supply rate, H₂O molecules are present on the surface. After a transitional period, σ_0 approaches an equilibrium value

$$\sigma_0(t = \infty) = \frac{s}{\frac{1}{2\tau} + \frac{\delta}{\theta}}. \quad (14)$$

For short times, $\sigma_0(t) = st$.

[30] The solution to the diffusion equation with the boundary condition $\rho(0, t) = \mu \sigma_0(\infty)/\ell$ can be found as follows [e.g., Strauss, 1992]. Take $\rho(z, t) = \tilde{\rho}(z, t) + \mu \sigma_0(\infty)/\ell$, then $\tilde{\rho}$ also satisfies the diffusion equation and has the boundary condition $\tilde{\rho}(0, t) = 0$ and the initial condition $\tilde{\rho}(z, 0) = -\mu \sigma_0(\infty)/\ell$ for $z > 0$. Using the reflection method, the solution can be obtained as

$$\begin{aligned} \tilde{\rho}(x, t) &= -\frac{1}{\sqrt{4\pi Dt}} \int_0^\infty dy \left[e^{-\frac{(x-y)^2}{4Dt}} - e^{-\frac{(x+y)^2}{4Dt}} \right] \mu \frac{\sigma_0(\infty)}{\ell} \\ &= -\mu \frac{\sigma_0(\infty)}{\ell} \text{Erf} \left(x/\sqrt{4Dt} \right). \end{aligned}$$

Hence

$$\rho(z, t) = \mu \frac{\sigma_0(\infty)}{\ell} \left(1 - \text{Erf} \left(z/\sqrt{4Dt} \right) \right) \quad (15)$$

The total H₂O mass is

$$\begin{aligned} m &= \int_0^\infty dz \rho(z, t) = \mu \frac{\sigma_0(\infty)}{\ell} \sqrt{\frac{4Dt}{\pi}} \\ &= \sigma_0(\infty) \sqrt{\frac{2t}{\pi\tau}} \end{aligned} \quad (16)$$

For comparison, the total amount supplied is μst . The mean depth is

$$\langle z \rangle = \frac{\int_0^\infty dz z \rho(z, t)}{\int_0^\infty dz \rho(z, t)} = \sqrt{\pi Dt/4} = \ell \sqrt{\frac{\pi t}{8\tau}}. \quad (17)$$

For testing purposes, the solution is compared to statistical model calculations (described in section 3.1) in Figure 5. Indeed, the statistical simulations agree with the continuum solutions for $t \gg \tau$.

[31] Figure 6 shows the column integrated ground ice mass as a function of temperature, compared to the amount of H₂O supplied over 1 billion years. According to equation (16), m is independent of ℓ . There is a temperature for which the amount of subsurface H₂O is a maximum. At low temperature little H₂O accumulates, because the migration is so slow. At temperatures higher than the optimum the loss from the surface is so fast that few source molecules reside

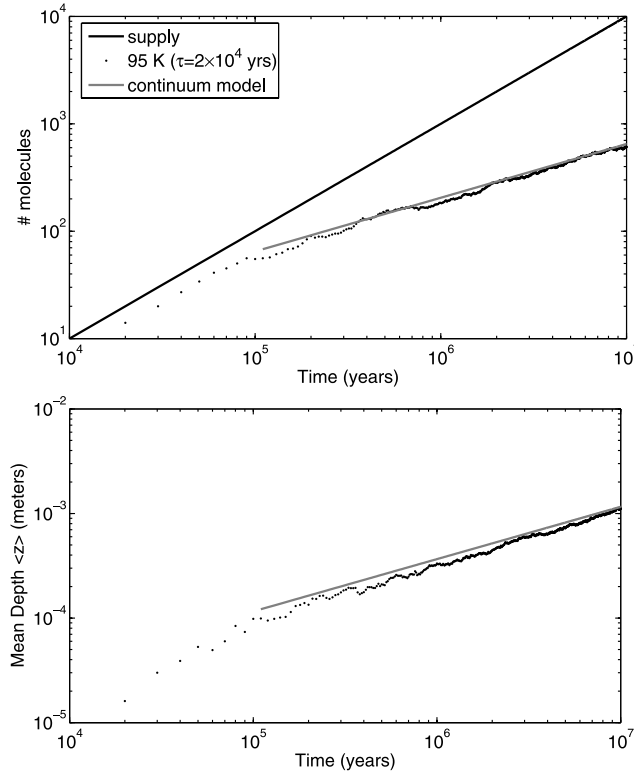


Figure 5. Comparison of statistical model calculations (dots) with analytical expressions (gray lines) for the total ice mass, equation (16), and the mean ice depth, equation (17), at a temperature of 95 K.

on the surface at any time. From differentiation of equation (16) with respect to τ , the maximum with respect to temperature is achieved for $1/(2\tau) = \delta/\theta$, that is, when the sublimation rate σ_0/τ is close to the space weathering rate $\delta\sigma_0/\theta$. The amount of subsurface H₂O depends on s and δ , but never exceeds $m = \mu\theta\sqrt{2t/(\pi\tau)}$, which it reaches when $\sigma_0(\infty) = \theta$, as can be seen from equation (16).

[32] The volume density of H₂O can be estimated by

$$\frac{m}{\langle z \rangle} = \frac{4}{\pi} \mu \frac{\sigma_0(\infty)}{\ell}$$

or by the density at average depth,

$$\rho(z, t) = \mu \frac{\sigma_0(\infty)}{\ell} (1 - \text{Erf}(\sqrt{\pi}/4)) \approx 0.5 \mu \frac{\sigma_0(\infty)}{\ell}.$$

Once σ_0 has assumed its equilibrium value, the H₂O molecules migrate deeper and deeper with time, but the overall density of H₂O remains unchanged. This density is on the order of $\mu\sigma_0/\ell$, and it reaches at most monolayer coverage, because $\sigma_0 \leq \theta$.

[33] Quantitatively, a monolayer cover corresponds to $\mu\theta/\ell \approx 4 \text{ g/m}^3$, on the order of a few ppm of the regolith density. Measurements of grain surface areas in lunar soil samples are on the order of $500 \text{ m}^2/\text{kg}$ [Heiken *et al.*, 1991]. Multiplied with the areal density of a monolayer of H₂O molecules, $\mu\theta$, this provides an H₂O fraction of a few

hundred ppm [Hodges, 2002]. This is substantially more than estimated from our one-dimensional model, due to actual surface to volume ratios of grains and the presence of fines in the lunar soils. We conclude that up to a few hundred ppm of H₂O could accumulate by this pathway. The maximum amount of H₂O that could be stored in this fashion is less than the minimum amount inferred by [Lawrence *et al.*, 2006]. Moreover, excess water is likely concentrated in areas smaller than the footprint of the Lunar Prospector neutron spectrometer, and the highest subsurface mixing ratios form only for optimal temperature and benign space weathering rates.

4.3. Initial Ice Cover

[34] Here we consider an initial, thick ice layer that may have formed during a giant comet impact. The exposed ice

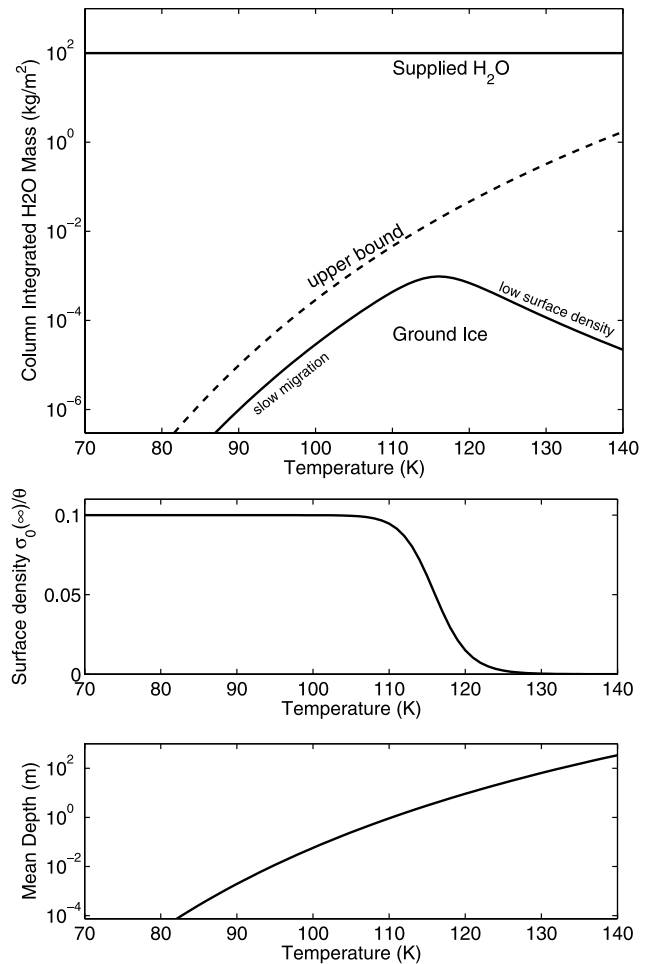


Figure 6. Ground ice accumulation after 1 billion years for a continuous supply of water. The assumed supply rate is $s\mu = 100 \text{ kg m}^{-2} \text{ Ga}^{-1}$. Since the supply is less than the destruction rate, no frost cover builds up on the surface, but a small fraction still migrates into the regolith. The upper bound (dash line) is an intrinsic limitation for this type of migration. These calculations conservatively assume no burial occurs, all molecules moving upward from the surface are permanently lost, and a pessimistic space weathering rate of $\mu\delta = 1000 \text{ kg m}^{-2} \text{ Ga}^{-1}$.

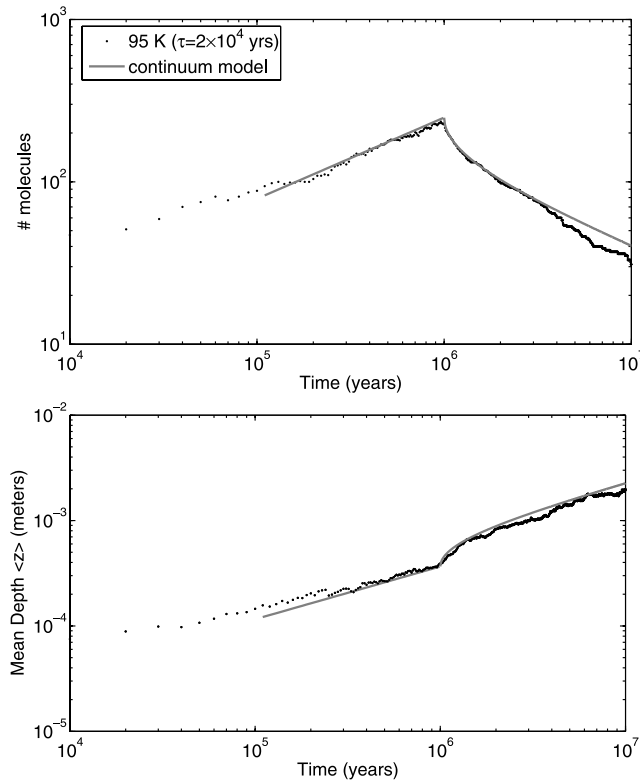


Figure 7. Comparison of statistical model calculations (dots) with analytical expressions (gray lines) for the total ice mass, equation (20), and the mean ice depth, equation (21), for a temperature of 95 K. The ice cover disappears after 10^6 years.

layer disappears after a time t_0 , due to losses, but some of the subsurface H₂O that accumulates during this time will last beyond t_0 .

[35] The upper boundary condition is $\rho(0, t) = \mu\theta/\ell$ as long as the ice layer is present, and $\rho(0, t) = 0$ afterward. For constant surface density, we can reuse result (15) from the previous section, but replace $\sigma_0(\infty)$ with θ ,

$$\rho(z, t) = \mu \frac{\theta}{\ell} \left[1 - \operatorname{Erf} \left(\frac{z}{\sqrt{4Dt}} \right) \right] \quad \text{for } t \leq t_0 \quad (18)$$

Integrated over depth, this yields the total ground ice mass for as long as an ice cover is present,

$$m = \mu \frac{\theta}{\ell} \sqrt{\frac{4Dt}{\pi}} = \mu\theta \sqrt{\frac{2t}{\pi\tau}} \quad \text{for } t \leq t_0 \quad (19)$$

The mean depth is the same as in equation (17).

[36] After the ice cover is lost, we obtain the solution by using as initial condition the final density distribution $\rho(z, t_0)$ from (18) and again employ the method of reflected sources,

$$\rho(z, t) = \frac{1}{\sqrt{4\pi Dt}} \int_0^\infty dy \left[e^{-\frac{(z-y)^2}{4D(t-t_0)}} - e^{-\frac{(z+y)^2}{4D(t-t_0)}} \right] \rho(y, t_0)$$

Although this integral cannot be carried out explicitly, it is possible to obtain the total mass by swapping the integration variables y and z .

$$\begin{aligned} m &= \frac{\mu\theta}{\ell} \int_0^\infty dy \operatorname{Erf} \left(\frac{y}{\sqrt{4D(t-t_0)}} \right) \left[1 - \operatorname{Erf} \left(\frac{y}{\sqrt{4Dt_0}} \right) \right] \\ &= \frac{\mu\theta}{\ell} \sqrt{\frac{4D}{\pi}} (\sqrt{t} - \sqrt{t-t_0}) \\ &= \mu\theta \sqrt{\frac{2}{\pi\tau}} (\sqrt{t} - \sqrt{t-t_0}) \quad \text{for } t \geq t_0 \end{aligned} \quad (20)$$

For $t \gg t_0$, when the cover lasted a relatively short period, $m \rightarrow \mu\theta t_0 / \sqrt{2\pi\tau t}$. In this case, the total remaining H₂O mass is proportional to the duration t_0 of the ice cover.

[37] In the same way, by swapping integrals, we obtain the mean depth

$$\begin{aligned} \langle z \rangle &= \sqrt{\frac{D\pi}{4}} \frac{t_0}{\sqrt{t} - \sqrt{t-t_0}} \\ &= \ell \sqrt{\frac{\pi}{8\tau}} \frac{t_0}{\sqrt{t} - \sqrt{t-t_0}} \quad \text{for } t \geq t_0 \end{aligned} \quad (21)$$

[38] Figure 7 shows again a comparison of statistical model calculations for verification purposes. In this comparison θ equals 40 molecules.

[39] Figure 8 shows the column integrated H₂O mass as a function of temperature, equation (20), compared to the amount of H₂O in the initial ice layer. The assumed initial ice cover is $M = 100 \text{ kg/m}^2$, approximately a 10 cm thick layer, and this mass is equivalent to what is delivered to the cold trap in Figure 6 over the same total time period of 1 billion years. The duration of the ice cover is calculated from δ , τ' , and M , according to $M = \mu(\theta/\tau' + \delta) t_0$. Here, τ' corresponds to the molecular bond in the ice layer, which can differ from the bond between the migrating H₂O molecules and the regolith grain surfaces. But we do eventually assume $\tau' = \tau$. The maximum amount of subsurface H₂O for any combination of weathering rate and initial ice thickness is obtained when the ice cover lasts until the present, $m = \mu\theta\sqrt{2t}/(\pi\tau)$ from equation (19), and is indicated by a dash line in Figure 8.

[40] The volume density of H₂O can be estimated by

$$\frac{m}{\langle z \rangle} = \frac{4}{\pi} \mu \frac{\theta}{\ell} \left(\sqrt{\frac{t}{t_0}} - \sqrt{\frac{t}{t_0} - 1} \right)^2.$$

The expression in parenthesis is always ≤ 1 . Hence the maximum H₂O density corresponds to monolayer coated grains, the same as described at the end of section 4.2.

5. Discussion

[41] Meteorite impacts lead to turnover and burial of regolith. This does not necessarily destroy the ice and may in fact protect it [Arnold, 1979], but quantitative estimates of diffusive migration are only relevant if it proceeds faster than the turnover or burial. Figure 9 shows the mean ice depth from equation (17) for several temperatures in comparison with estimates of the gardening depth [Heiken et al., 1991; Arnold, 1975]. For temperatures above

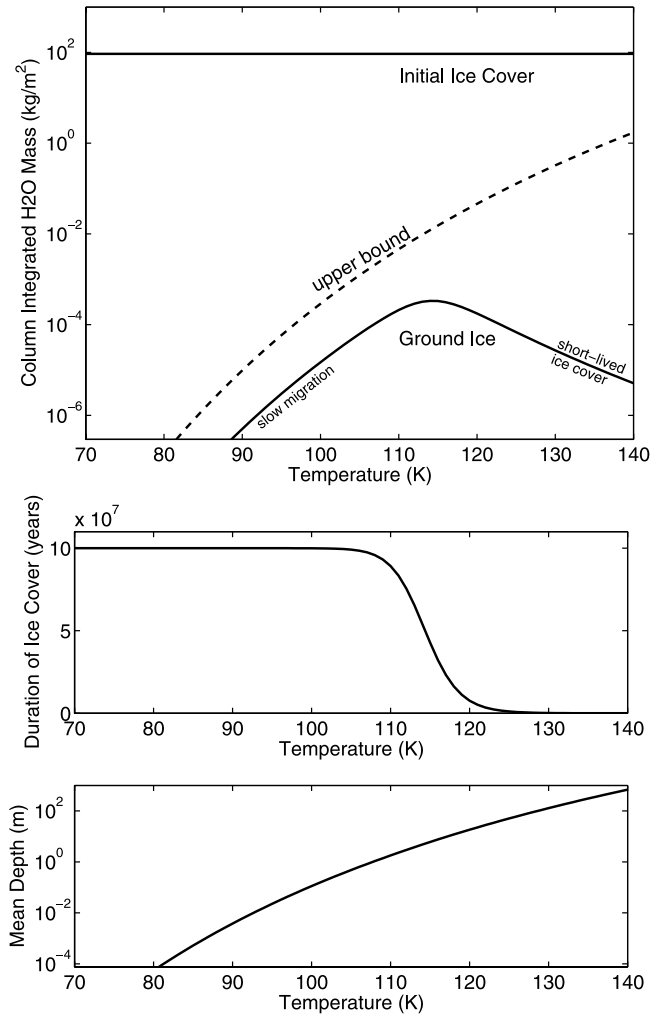


Figure 8. Ground ice accumulation after 1 billion years for an initial ice cover. The cover disappears due to losses, but a small fraction of H₂O remains inside the regolith. The upper bound (dash line) cannot be exceeded for any input parameters. The bottom two panels show mean depth $\langle z \rangle$ and duration of the ice cover t_0 . Mean depths less than ℓ are not shown.

~110 K (using residence times for crystalline ice), gardening never significantly affects the subsurface migration of ice.

[42] Radiation destroys molecules on the surface of the cold trap before they can migrate downward. The existence of a condensation coefficient $\alpha < 1$ may be important, because some molecules that land on cold areas will jump to protected pores without spending time on the surface. In hiding places not directly exposed to space weathering, molecules would experience substantially lower destruction rates. We have not considered this effect in our model calculations, but it may enhance the amount of H₂O in the subsurface under the scenario discussed in section 4.2.

[43] The binding energy of molecules adsorbed to the regolith differs from that in ice. The sublimation enthalpy of crystalline ice is 51 kJ/mol, that of amorphous ice formed by deposition at low temperature is 0.45 eV or 43 kJ/mol

[Sack and Baragiola, 1993]. de Leeuw et al. [2000] report adsorption energies for H₂O on forsterite surfaces of 100–172 kJ/mol. The adsorption energy does not determine the residence time by itself. The average time of stay τ of the molecule on the surface of a substrate is

$$\tau = \frac{1}{\nu} \exp\left(\frac{Q}{kT}\right) \quad (22)$$

where ν approximately corresponds to the vibrational frequency of the bond between the H₂O molecule and the substrate surface, typically 10^{12} – 10^{14} Hz, and Q is the energy of adsorption [Adamson, 1982; Atkins, 1986]. We have not found values for ν for H₂O on olivine at cold temperatures in the literature.

[44] We do not have the appropriate data to quantitatively describe the residence times of adsorbed molecules. Hence we emphasized general results and equations. The residence time for crystalline ice is used in example cases.

[45] A chemisorbed or physically strongly adsorbed layer of H₂O molecules may exist on lunar grains that is stable indefinitely [Hodges, 2002; Cocks et al., 2002]. Since the stability of this layer is so strong, it may preexist, and our calculations only consider the volatile water.

[46] The appropriate residence time for the type of migration process considered in sections 3.1 and 4.2 is the adsorption of H₂O on a substrate. It is possible to imagine situations where changes in binding energies with layer are important, but when the first layer is extremely strongly adsorbed and preexistent, our results remain valid after they are adjusted for more accurate values of τ .

[47] The upper bound on H₂O accumulation is independent of the residence times, because it corresponds to the mass of a monolayer, which in turn is determined by the available surface area. This maximum mass should equal the amount that is chemisorbed, essentially up to doubling the possible hydrogen content.

[48] A further complication arises when an ice layer, with its binding energy, faces regolith grains with a different finite binding energy, as in sections 4.1 and 4.3, because surface concentrations can compensate for differences in residence time to achieve a flux balance. The loss rate of

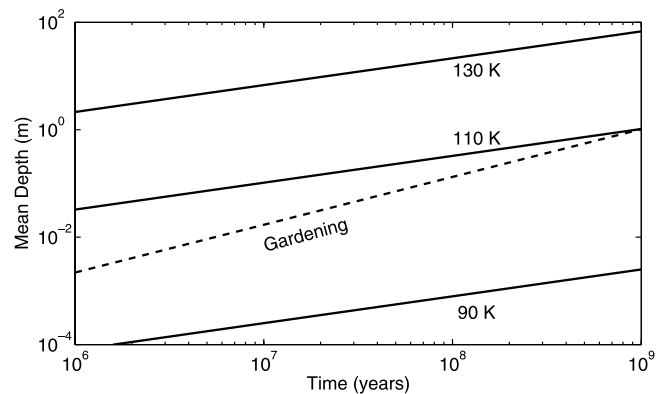


Figure 9. Mean depth $\langle z \rangle$ of ground ice from equation (17) compared to the lunar gardening depth [Arnold, 1975] as a function of time.

buried ice is still governed by the residence time of molecules in ice.

6. Multilayer Coverage

[49] When a layer of H₂O covers up an earlier layer, not every molecule is free to escape. We now develop equations for multilayer coverage, which are especially relevant for time varying temperatures. We imagine again a one-dimensional model with discrete sites spaced by a distance $\ell = 75 \mu\text{m}$, which represent a typical grain size diameter.

[50] The fraction of a site's area coated with H₂O is denoted with c_n , which ranges from 0 to 1. For a site at depth $z_n = n\ell$, the outward flux is $c_n E_n$, while the received flux from both sides is $(c_{n-1} E_{n-1} + c_{n+1} E_{n+1})/2$. The areal density σ_n is described by

$$\frac{\partial \sigma_n}{\partial t} = \frac{1}{2} c_{n-1} E_{n-1} - c_n E_n + \frac{1}{2} c_{n+1} E_{n+1} \quad (23)$$

$$c_n = \min(\sigma_n/\theta, 1) \quad (24)$$

[51] In a continuum formulation, we can write (23) and (24) in terms of a volume mass density $\rho = \mu\sigma/\ell$,

$$\frac{\partial \rho}{\partial t} = \mu \frac{\ell}{2} \frac{\partial^2}{\partial z^2} (cE) \quad (25)$$

$$c = \min\left(1, \frac{\rho\ell}{\mu\theta}\right) \quad (26)$$

Here, $c(z, t)$ is a spatially averaged c_n . The associated mass flux is $J = -\mu(\ell/2)\partial(cE)/\partial z$.

[52] When the temperature is constant with depth and $c \leq 1$, the evaporation rate $E = \theta/\tau$ can be pulled out of the derivative in (25), and what remains is a diffusion equation for the coverage:

$$\frac{\partial c}{\partial t} = \frac{\ell^2}{2\tau} \frac{\partial^2 c}{\partial z^2}$$

Since the same expression also holds for $\rho = \mu c\theta/\ell$, this reproduces equation (8). This is the diffusive migration investigated in sections 3 to 5. Another special case of equations (25) and (26) is $c = 1$,

$$\frac{\partial \rho}{\partial t} = \mu \frac{\ell}{2} \frac{\partial^2 E}{\partial z^2} \quad (27)$$

The right-hand side vanishes when the temperature is constant with depth.

[53] The flux may be decomposed as

$$J = -\mu \frac{\ell}{2} \left(E \frac{\partial c}{\partial z} + c \frac{\partial E}{\partial z} \right). \quad (28)$$

Transport can be caused by differences in surface concentrations c or by differences in sublimation rates E . At constant temperature, only the concentration driven

migration occurs, while geothermal heat and temperature oscillations are causes of the second form of transport. With these equations at hand, we can now proceed to study migration when the sublimation rate E changes with time and depth.

7. Pumping Effect

[54] Transport of water can result from differences in sublimation rates with depth. This does not require a change of mean temperature with depth. Time integration of (27) for temperature oscillations around a constant mean yields $\rho = t\mu(\ell/2)(\partial^2 \langle E \rangle / \partial z^2)$, where $\langle E \rangle$ is the sublimation rate averaged over time. Since the sublimation rate depends nonlinearly on temperature, a time varying temperature, even when periodic, causes pumping of molecules to depth. Due to the convex shape of P_v , $\langle E \rangle$ is larger for larger temperature amplitudes. Diurnal temperature amplitudes decay with depth and $\langle E(T) \rangle$ therefore decreases with depth. The ground ice mass increases proportionally with time as long as there is an ice source on the surface.

[55] The temperature is modeled by a sinusoidally varying surface temperature: $T = T_m + T_a \exp(-z/\lambda) \sin(z/\lambda - \omega t) + gz$, which represents a solution to the heat conduction equation. Here, T_m is the mean temperature, T_a the temperature amplitude, λ the thermal skin depth (assumed 0.1 m), ω the diurnal period (of the Moon), and g the geothermal gradient (assumed 1 K/m). Reality will have a more complex temperature history and depth dependence [Salvail and Fanale, 1994; Vasavada et al., 1999], but our model temperature contains the essential ingredients.

[56] Experimentally measured sublimation rates for H₂O ice were shown in Figure 2. We use the rates of Sack and Baragiola [1993], extrapolated to lower temperatures with constant enthalpy.

[57] Three levels of models are used in our simulations. The first simulates discrete sites and a time varying temperature and uses equations (23) and (24). This requires time steps much shorter than one month. The second level of model uses time-averaged evaporation rates in (23), leading to much faster simulations. The third and fastest type of model solves the continuum equations (25) and (26), which allows for a spatial resolution coarser than ℓ . We have compared results from each of these three models with each other for verification, and only present results obtained with the last of these models here.

[58] Figure 10 shows the result of model calculations. Beginning with an ice cover and dry regolith, molecules migrate downward, and some of them remain in the subsurface after the ice cover has disappeared. There are four phases in the time evolution, as seen in Figure 10a. Initially, transport is dominated by diffusively migrating H₂O molecules (proportional to the square root of time), followed by a period when most mass is transferred by pumping (proportional with time). After the ice cover has disappeared, the ice-rich layer disperses rapidly, followed by a slow loss of the diffusively accumulated H₂O. Figure 10b shows snapshots of the depth distribution, with a clear bend seen between multilayer coverage and less than monolayer coverage. These simulations make clear that multiple layers of ice accumulate on grains through pumping. Figure 10c shows the maximum areal density, $\max_z \sigma/\theta$; it

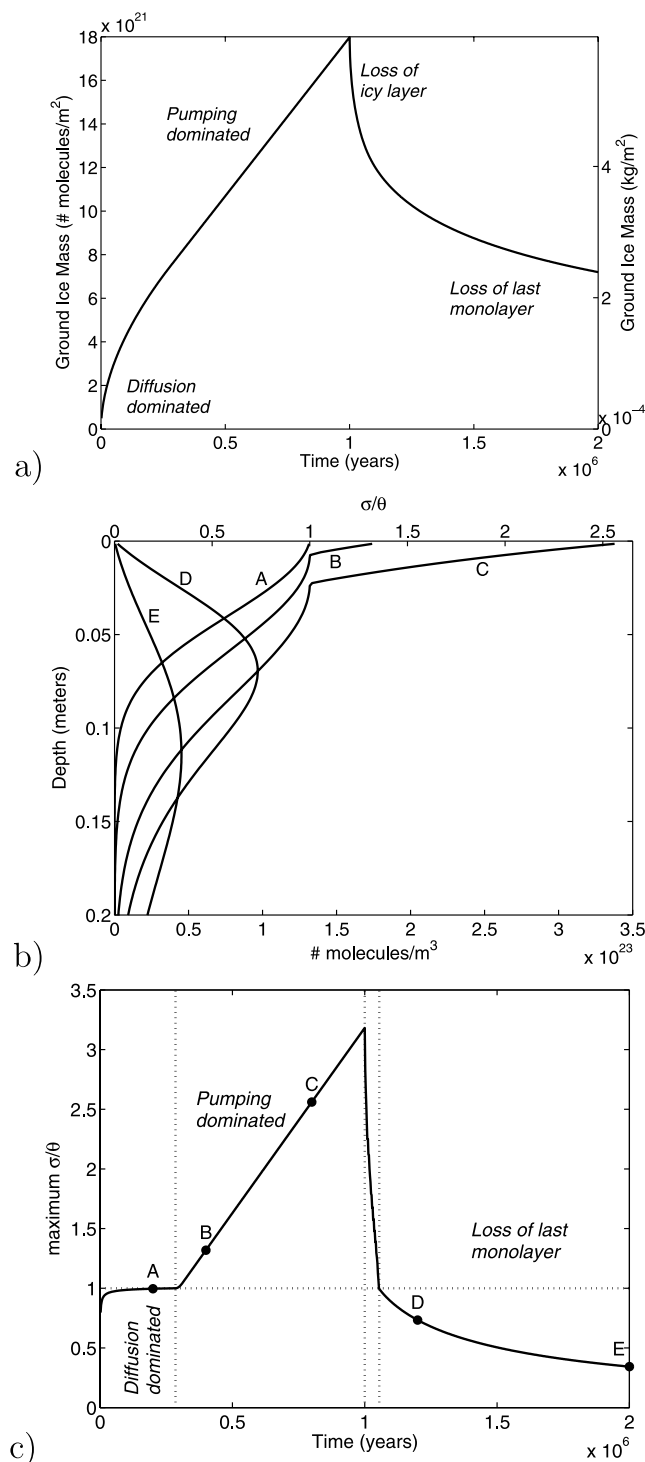


Figure 10. Numerical model calculations of H₂O migration into the lunar subsurface with an initial ice layer on the surface that disappears after 1 million years. The mean temperature is 110 K, and the amplitude is 5 K. (a) Column integrated ground ice mass as a function of time. (b) Instantaneous depth profiles of ice density. (c) Maximum number of molecular H₂O layers, $\max_z \sigma/\theta$, as a function of time. Vertical dotted lines separate the four phases of the time evolution. Dots mark the times of the 5 snapshots in Figure 10b.

can be used to precisely separate the four phases of the time evolution. Since the ground ice mass increases proportionally with time during the pumping dominated phase, large volume densities can accumulate when the ice cover lasts sufficiently long.

[59] Higher temperatures enhance the pumping, because absolute sublimation rates are higher, but they also reduce the lifetime of the ice cover. Hence the ground ice mass is again expected to be highest for an intermediate temperature.

8. Conclusions

[60] This paper investigated the migration of H₂O molecules in the lunar and Mercurian regolith by random hops. Among our general results are an expression for the effective diffusion coefficient of H₂O molecules (5) and a transport equation for subsurface migration (7). Transport with partial or multiple molecular layers is described by equations (25) and (26).

[61] The survival time of ice buried beneath porous regolith can be estimated with equation (11). The loss rate turns out to be equivalent to the Knudsen flux through a porous medium. The diffusive barrier reduces the ice loss, compared to the sublimation loss of exposed ice at the same temperature, roughly by a factor of molecule hop length divided by layer thickness.

[62] We then discussed two scenarios for subsurface accumulation of externally derived water at constant temperature. One assumes a gradual supply of water to the surface and the other an initial ice layer. Our calculations indicate that in an appropriate temperature range water molecules can travel into the regolith before they are destroyed. Higher temperatures lead to deeper burial, and the deeper burial leads to preservation during impact gardening. We find there is an optimum temperature which maximizes the subsurface H₂O content and an intrinsic limitation to the density of H₂O that can accumulate by this type of migration. The grain coverage is limited to less than one layer of volatile H₂O molecules, because differences in surface concentration are necessary for net transport of additional molecules. The process should lead to a small amount of H₂O, depending on the grain size probably up to a few hundred ppm in excess of what is chemisorbed and extremely strongly adsorbed. The most favorable temperatures are in the range 110–130 K, if assumed residence times are also characteristic for adsorption. Both charging scenarios work most efficiently for temperatures typical of areas permanently shaded from direct sunlight but with sunlit surfaces in their field of view.

[63] Temperature oscillations provide a qualitatively different pathway for molecule transport than described above, driven by differences in (average) sublimation rates. Although this mechanism can produce a higher density of ice in the subsurface, the ice-rich layer disappears rapidly after the ice cover is gone.

[64] We conclude that neither of the two pathways would create abundant ice reservoirs, unless there is an even more massive ice cover on top. However, the expectation is that, as long as H₂O is delivered to permanently shaded areas at all, a fraction remains, adsorbed in the uppermost regolith, not at the coldest temperatures but for temperatures that allow limited migration of water molecules.

[65] **Acknowledgments.** It is a pleasure to thank Paul Lucy, Marilena Stimpfl, and Ashwin Vasavada for insightful discussions. This material is based upon work supported by the National Aeronautics and Space Administration through the NASA Astrobiology Institute under Cooperative Agreement NNA04CC08A issued through the Office of Space Science.

References

- Adamson, A. (1982), *Physical Chemistry of Surfaces*, 4th ed., Wiley-Interscience, Hoboken, N. J.
- Arnold, J. R. (1975), Monte Carlo simulation of turnover processes in the lunar regolith, *Proc. Lunar Sci. Conf. 6th (2)*, 2375–2395.
- Arnold, J. R. (1979), Ice in the lunar polar regions, *J. Geophys. Res.*, *84*(B10), 5659–5667.
- Arnold, J. R. (1987), Ice at the lunar poles revisited (abstract), *Proc. Lunar Planet. Sci. Conf. 18th*, 29–30.
- Atkins, P. W. (1986), *Physical Chemistry*, 3rd ed., Oxford Univ. Press, New York.
- Bryson, C. E., V. Cazcarra, and L. L. Levenson (1974), Sublimation rates and vapor pressures of H₂O, CO₂, N₂O, and Xe, *J. Chem. Eng. Data*, *19*(2), 107–110.
- Butler, B. J. (1997), The migration of volatiles on the surfaces of Mercury and the Moon, *J. Geophys. Res.*, *102*(E8), 19,283–19,291.
- Butler, B. J., D. O. Muhleman, and M. A. Slade (1993), Mercury: Full-disk radar images and the detection and stability of ice at the North Pole, *J. Geophys. Res.*, *98*(E8), 15,003–15,024.
- Campbell, B. A., D. B. Campbell, A. A. H. J. F. Chandler, M. C. Nolan, and P. J. Perillat (2003), Radar imaging of the lunar poles, *Nature*, *426*, 137–138.
- Cocks, F., P. Klenk, S. Watkins, W. Simmons, J. Cocks, E. Cocks, and J. Sussingham (2002), Lunar ice: Adsorbed water on subsurface polar dust, *Icarus*, *160*, 386–397.
- Crider, D., and R. Vondrak (2003a), Space weathering of ice layers in lunar cold traps, *Adv. Space Res.*, *31*(11), 2293–2298.
- Crider, D. H., and R. R. Vondrak (2003b), Space weathering effects on lunar cold trap deposits, *J. Geophys. Res.*, *108*(E7), 5079, doi:10.1029/2002JE002030.
- de Leeuw, N., S. Parker, C. Catlow, and G. Price (2000), Modelling the effect of water on the surface structure and stability of forsterite, *Phys. Chem. Minerals*, *27*, 332–341.
- Fanale, F. P., and J. R. Salvail (1984), An idealized short-period comet model: Surface insolation, H₂O flux, dust flux, and mantle convection, *Icarus*, *60*(3), 476–511.
- Feldman, W., S. Maurice, B. B. A. B. Binder, R. Elphic, and D. Lawrence (1998), Fluxes of fast and epithermal neutrons from lunar prospector: Evidence for water ice at the lunar poles, *Science*, *281*(5382), 1496–1500.
- Harmon, J. K., M. A. Slade, R. A. Velez, A. Crespo, M. J. Dryer, and J. M. Johnson (1994), Radar mapping of Mercury's polar anomalies, *Nature*, *369*, 213–215, doi:10.1038/369213a0.
- Harmon, J. K., P. J. Perillat, and M. A. Slade (2001), High-resolution radar imaging of Mercury's north pole, *Icarus*, *149*, 1–15, doi:10.1006/icar.2000.6544.
- Haynes, D. R., N. J. Tro, and S. M. George (1992), Condensation and evaporation of H₂O on ice surfaces, *J. Phys. Chem.*, *96*, 8502–8509.
- Heiken, G. H., D. T. Vaniman, and B. M. French (Eds.) (1991), *Lunar Sourcebook: A User's Guide to the Moon*, 753 pp., Cambridge Univ. Press, New York.
- Hodges, R. R., Jr. (2002), Ice in the lunar polar regions revisited, *J. Geophys. Res.*, *107*(E2), 5011, doi:10.1029/2000JE001491.
- Killen, R. M. (2002), Source and maintenance of the argon atmospheres of Mercury and the Moon, *Meteorit. Planet. Sci.*, *37*, 1223–1231.
- Langmuir, I. (1913), The vapor pressure of metallic tungsten, *Phys. Rev.*, *2*(5), 329–342.
- Lanzerotti, L., W. L. Brown, and R. E. Johnson (1981), Ice in the polar regions of the moon, *J. Geophys. Res.*, *86*, 3949–3950.
- Lawrence, D. J., W. C. Feldman, R. C. Elphic, J. J. Hagerty, S. Maurice, G. W. McKinney, and T. H. Prettyman (2006), Improved modeling of Lunar Prospector neutron spectrometer data: Implications for hydrogen deposits at the lunar poles, *J. Geophys. Res.*, *111*, E08001, doi:10.1029/2005JE002637.
- Morgan, T., and D. Shemansky (1991), Limits to the lunar atmosphere, *J. Geophys. Res.*, *96*(A2), 1351–1367.
- Moses, J. I., K. Rawlins, K. Zahnle, and L. Dones (1999), External sources of water for Mercury's putative ice deposits, *Icarus*, *137*, 197–221, doi:10.1006/icar.1998.6036.
- Nozette, S., C. L. Lichtenberg, P. D. Spudis, R. Bonner, W. Ort, E. Malaret, M. Robinson, and E. M. Shoemaker (1996), The Clementine Bistatic Radar Experiment, *Science*, *274*, 1495–1498.
- Sack, N. J., and R. A. Baragiola (1993), Sublimation of vapor-deposited water ice below 170 K, and its dependence on growth conditions, *Phys. Rev. B*, *48*(14), 9973–9978.
- Salvail, J. R., and F. P. Fanale (1994), Near-surface ice on Mercury and the Moon: A topographic thermal model, *Icarus*, *111*, 441–455.
- Slade, M. A., B. J. Butler, and D. O. Muhleman (1992), Mercury radar imaging—Evidence for polar ice, *Science*, *258*, 635–640.
- Speedy, R. J., P. G. Debenedetti, R. S. Smith, C. Huang, and B. D. Kay (1996), The evaporation rate, free energy, and entropy of amorphous water at 150 K, *J. Chem. Phys.*, *105*(1), 240–244.
- Stacy, N., D. Campbell, and P. Ford (1997), Arecibo radar mapping of the lunar poles: A search for ice deposits, *Science*, *276*, 1527–1530.
- Strauss, W. A. (1992), *Partial Differential Equations: An Introduction*, John Wiley, Hoboken, N. J.
- Svitek, T., and B. Murray (1988), Lunar polar ice—A reappraisal, *Proc. Lunar Planet. Sci. Conf. 19th*, Abstract 1160.
- Vasavada, A. R., D. A. Paige, and S. E. Wood (1999), Near-surface temperatures on Mercury and the Moon and the stability of polar ice deposits, *Icarus*, *141*, 179–193.
- Vondrak, R., and D. Crider (2003), Ice at the lunar poles, *Am. Sci.*, *91*(4), 322–329.
- Ward, W. (1975), Past orientation of the lunar spin axis, *Science*, *189*, 377–379.
- Washburn, E., et al. (Eds.) (2003), *International Critical Tables of Numerical Data, Physics, Chemistry and Technology*, 1st electron. ed., Knovel, Norwich, N. Y.
- Watson, K., B. C. Murray, and H. Brown (1961a), On the possible presence of ice on the Moon, *J. Geophys. Res.*, *66*(5), 1598–1600.
- Watson, K., B. C. Murray, and H. Brown (1961b), The behavior of volatiles on the lunar surface, *J. Geophys. Res.*, *66*(9), 3033–3045.

N. Schorghofer, Institute for Astronomy, 2680 Woodlawn Drive, Honolulu, HI 96822, USA. (norbert@hawaii.edu)

G. J. Taylor, Hawaii Institute of Geophysics and Planetology, University of Hawaii, 1680 East-West Road, Honolulu, HI 96822, USA. (gjtaylor@higp.hawaii.edu)